

Examining evapotranspiration trends in Africa

Michael Marshall · Christopher Funk ·
Joel Michaelsen

Received: 10 December 2010 / Accepted: 16 January 2012 / Published online: 5 February 2012
© Springer-Verlag 2012

Abstract Surface temperatures are projected to increase 3–4°C over much of Africa by the end of the 21st century. Precipitation projections are less certain, but the most plausible scenario given by the Intergovernmental Panel on Climate Change (IPCC) is that the Sahel and East Africa will experience modest increases (~5%) in precipitation by the end of the 21st century. Evapotranspiration (E_a) is an important component of the water, energy, and biogeochemical cycles that impact several climate properties, processes, and feedbacks. The interaction of E_a with climate change drivers remains relatively unexplored in Africa. In this paper, we examine the trends in E_a , precipitation (P), daily maximum temperature (T_{\max}), and daily minimum temperature (T_{\min}) on a seasonal basis using a 31 year time series of variable infiltration capacity (VIC) land surface model (LSM) E_a . The VIC model captured the magnitude, variability, and structure of observed runoff better than other LSMs and a hybrid model included in the analysis. In addition, we examine the inter-correlations of E_a , P , T_{\max} , and T_{\min} to determine relationships and potential feedbacks. Unlike many IPCC climate change simulations, the historical analysis reveals substantial drying over much of the Sahel and East Africa

during the primary growing season. In the western Sahel, large increases in daily maximum temperature appear linked to E_a declines, despite modest rainfall recovery. The decline in E_a and latent heating in this region could lead to increased sensible heating and surface temperature, thus establishing a possible positive feedback between E_a and surface temperature.

Keywords Evapotranspiration · Climate change · Land surface models · VIC · Africa

1 Introduction

Evapotranspiration is an important component of the water, energy, and biogeochemical cycles that impact several climate properties, processes, and feedbacks that relate to landcover and phenological change. The timing and extent of a major heat wave across Europe in 2003 for example, lead to an increase in sensible heating and decline in evaporative cooling, which further amplified sensible heating and surface temperatures during the normal growing season when drought conditions were most severe (Fischer et al. 2007). Evapotranspiration is limited by soil moisture supply and atmospheric moisture demand. The former is largely linked to precipitation, while the latter relates to net radiation and advection which are impacted by surface and atmospheric temperature (Law et al. 2002). The coupling of evapotranspiration, temperature, and precipitation is particularly pronounced in moisture-limited sub-tropical regions at the interface between wet (monsoonal) and dry climate regimes (Koster et al. 2004). Notably, runoff (Q) has been declining throughout many sub-tropical regions during the primary growing season (Huntington 2006). These declines have been attributed to

M. Marshall (✉) · J. Michaelsen
Department of Geography, Climate Hazards Group,
University of California Santa Barbara, Santa Barbara, CA, USA
e-mail: marshall@geog.ucsb.edu

J. Michaelsen
e-mail: joel@geog.ucsb.edu

C. Funk
US Geological Survey Earth Resources Observation
and Science (EROS) Center, Department of Geography,
University of California Santa Barbara,
Santa Barbara, CA, USA
e-mail: cfunk@usgs.gov

decreasing precipitation and increasing temperature which have caused soil moisture to decline and atmospheric demand to increase. Despite increases in atmospheric demand, or potential evapotranspiration (E_p), soil moisture deficits in subtropical regions have caused evapotranspiration (E_a) rates to decline in recent decades. In fact, steeply declining soil moisture in subtropical Africa and Australia has been a major contributor to a global decline in annual E_a of ~ 10 mm since the 1997–1998 El Niño event (Jung et al. 2010). Global E_a declines correspond to simulated losses in net primary production of up to 21 gC/m²/year in some areas, reducing global carbon sequestration and increasing surface heating due to desertification and increased sensible heating (Zhao and Running 2010). Understanding the magnitude, timing, and variability of changes in E_a and its connection to temperature and precipitation changes in the sub-tropics and tropics is therefore a regional concern with global implications.

A key research objective is to determine how trends in the supply and demand side of moisture availability have impacted vegetation (Allen et al. 2010; Lobell and Burke 2010). Studies which analyze the interaction of regional land surface climate and E_a in Africa have focused on the relationship between E_a proxies, such as soil moisture and plant phenology, to precipitation (P). Although surface temperature– E_a relationships exist in Africa, namely the negative relationship between E_a and atmospheric demand as demonstrated with simulated data (Koster et al. 2006), regional analysis of this relationship remains unexplored. In the Sahel, increases in soil moisture (E_a) can establish a positive feedback, in which wetter soils produce increased atmospheric instability and moisture convergence, leading to increased P (Douville 2002). In southern Africa, on the other hand, a negative feedback between E_a and P has been observed, in which increased E_a acts to lower sensible heat thus enhancing atmospheric stability and subsidence (Cook et al. 2006).

For Africa, a vast body of literature exists, beginning with Nicholson et al. (1990), that explores trends in P and the normalized difference vegetation index (NDVI). NDVI is derived from red and infrared wavelengths captured by remote sensors. These wavelengths give a relative measure of the photosynthetic capacity of plants (Sellers et al. 1996a). Increases in NDVI typically lag P by 1–2 months, due to the accumulated response of plants to root zone moisture in semi-arid areas where vegetation is sensitive to interannual rainfall fluctuations (Camberlin et al. 2007). Using NDVI, increases in vegetation biomass have been attributed to increases in precipitation over much of the Sahel during the primary growing season (Philippon et al. 2007), while decreasing trends in NDVI have been attributed to the intensification of the El Niño Southern Oscillation (ENSO) in southern Africa (Anyamba and Eastman

1996). Although the magnitude and extent of the former, typically referred to as the “re-greening of the Sahel” is uncertain (Giannini et al. 2008), several authors have attributed this change in part to a positive feedback between soil moisture and P (Giannini et al. 2003; Wang and Eltahir 2000; Zeng 2003; Zeng and Neelin 2000; Zeng et al. 1999). A time series analysis of E_a in Africa could improve upon these studies by providing a quantifiable measure of a regional water balance component that is more tightly coupled to the atmosphere than soil moisture.

The purpose of this study is to explore trends in the phase (timing) and magnitude of E_a in Africa during the past 31 years and to relate these changes to trends in P and surface temperature as proxies for surface moisture storage and atmospheric moisture demand, respectively. It should be stressed that this analysis is based on simulated data, because it has been difficult for the climate community to agree on a multimodal ensemble mean that characterizes all aspects of climate at the interface of the Sahel and Saharan desert (Xue et al. 2010). Land surface models (LSMs) and hybrid models are used to simulate and explore these trends. LSMs are defined here as those models that yield global estimates of the land surface state and fluxes by interactively incorporating global-scale, ground-based and remote sensing derived soil, vegetation, and atmospheric forcing data. The ground-based and remote sensing data are used to reduce bias in synthesizing the reanalysis data. The hybrid models incorporate a dynamic green canopy (transpiration) component defined in Fisher et al. (2008), which is driven by time series of vegetation indices that may be more appropriate in semi-arid regions where the variability in photosynthesis is not adequately captured using leaf area index (LAI) monthly means (DehghaniSanij et al. 2004). LSM and hybrid model E_a over a 31 year period is used to meet the following objectives: (1) identification of an LSM or hybrid model that best represents the timing and magnitude of moisture fluxes in Africa; (2) seasonal trend analysis of E_a and relation to trends in surface temperature and P; and (3) trend analysis of the timing of peak E_a .

2 Methods

2.1 Land surface models

The LSMs used in this paper are part of the global land data assimilation system (GLDAS) (Rodell et al. 2004). GLDAS integrates several climate reanalysis, remote sensing, and observation datasets to drive the LSMs which in turn provide further information on soil moisture and latent heat and sensible heat flux. Forcing and output data is provided by the National Aeronautics and Space

Administration Global Goddard Space Flight Center Hydrology Branch (<http://daac.gsfc.nasa.gov/hydrology>). The parameterization data include the bias-corrected European Center for Medium-Range Weather Forecasts (ECMWF) Reanalysis from 1979 to 1993 and National Center for Atmospheric Research (NCAR) Reanalysis from 1994 to 1999 (Berg et al. 2003), NOAA global data assimilation system (GDAS) atmospheric analysis fields (Derber et al. 1991) for 2000, and from 2001 to 2009 a combination of National Oceanic and Atmospheric Administration (NOAA) GDAS atmospheric analysis fields, climate prediction center merged analysis of precipitation (CMAP) fields (Xie and Arkin 1997), and radiation fields derived from observed incoming radiation using the method of the Air Force Weather Agency's AGRicultural METeorological modeling system (Idso 1981; Shapiro 1987). The forcing data are synthesized using various ground-based and remote sensing data and assimilation techniques are used to improve model accuracy, resolution, and consistency. The process yields a 31-year (1979–2009) global monthly time series of E_a at 1.0° resolution. The estimated E_a from three of the LSMs were chosen for comparison in this paper, including the Common Land Model Version 2 (CLM), Noah, and the variable infiltration capacity model (VIC).

2.1.1 CLM

The CLM was developed from collaboration of a community of scientists and improves on three existing LSMs by combining the best elements from each. These include the NCAR LSM (Bonan 1998), the biosphere–atmosphere transfer scheme (BATS) (Dickenson et al. 1986), and the LSM of the Institute of Atmospheric Physics of the Chinese Academy of Sciences (Dai and Zeng 1997). The model employs a single column soil–vegetation–atmosphere transfer (SVAT) scheme, discretized using finite-difference methods and split-hybrid (energy and water balance) temporal integration (Dai et al. 2003). The vegetation component consists of one layer parameterized using NCAR LSM photosynthesis–stomatal resistance which is based on the semi-empirical Ball version described in Sellers et al. (1996b). Large negative biases in CLM Q due to overestimation of E_a have been observed in tropical basins, most notably the Amazon basin (Dickinson et al. 2006), and have been attributed primarily to inaccurate parameterization data and secondly to a poor soil layering scheme (Qian et al. 2006).

The E_a component used in CLM, as with the other LSMs used in this paper, consists of three terms: evaporation from bare soil (E_s), wet canopy evaporation (E_w), and transpiration (E_t).

$$E_a = \underbrace{\frac{\rho c_p f_{\text{wet}} (e_{\text{sat}} - e_a)}{\gamma}}_{E_w} + \underbrace{\frac{\rho c_p (e_{\text{sat}} - e_a)}{\gamma}}_{E_s} + \underbrace{\frac{\rho c_p (1 - f_{\text{wet}}) (e_{\text{sat}} - e_a)}{\gamma}}_{E_t} \left(\frac{1}{R_a + R_s^{\text{sun}}} + \frac{1}{R_a + R_s^{\text{sha}}} \right) \quad (1)$$

where ρ is air density, γ is the psychrometric constant, R_a is the aerodynamic resistance bounded by the reference height and free atmosphere, R_{soil} is the bare soil resistance constrained by dimensionless soil wetness function defined in Lee and Pielke (1992), R_s^{sun} is the stomatal resistance for the sunlight fraction of the canopy, R_s^{sha} is the stomatal resistance for the shaded fraction of the canopy, f_{wet} is the fraction of the canopy that is wet, e_{soil} is the vapor pressure of the soil defined in Philip (1957), e_{sat} is the saturation vapor pressure, e_a is the vapor pressure at reference height, and c_p is the specific heat of air. E_t is a function of Penman–Monteith E_p constrained by three resistance terms (Bonan 1996). Stomatal resistance is computed at the leaf level for the sunlight (shortwave energy flux) and shaded (longwave energy flux) which is then scaled to the canopy scale using LAI.

2.1.2 Noah

The National Centers for Environmental Protection, Oregon State University, Air Force, and Hydrologic Research Lab (Noah) model was first developed in the early 1990's through collaboration between government and private institutions. It has gone through a series of improvements, including the introduction of a canopy resistance component and an increase in the number of soil layers (Chen et al. 1996), introduction of snowpack and frozen ground physics (Koren et al. 1999), variable roughness length dependent on the Reynold's number (Chen et al. 1997), implementation of a soil thermal model and a vegetation fraction derived from remote sensing climatology (Betts et al. 1997), and a non-linear (quadratic) soil evaporation function (Ek et al. 2003). The model uses a single column SVAT transfer scheme, discretized using finite-difference methods and a Crank–Nicholson (energy balance) temporal integration scheme. The vegetation component consists of one layer adapted from the Jacquemin and Noilhan (1990) photosynthesis–stomatal resistance model. The model tends to have a low-level warm season bias, which has been attributed to under-prediction of the vegetation fraction of the transpiration component of E_a . This bias tends to be stronger in semi-arid areas where plant phenology is highly variable (Hogue et al. 2005).

The Noah component of E_a , unlike CLM, constrains E_p using water storage terms and is therefore dependent primarily on P instead of vapor pressure. Bare soil evaporation, originally parameterized using a demand–supply approach similar to CLM, was later adapted after Mahfouf and Noilhan (1991) and now only relies on soil moisture. E_t and E_w are functions of the intercepted canopy water content (W_c), which is a residual of the water balance:

$$E_a = \left\{ \underbrace{(1 - f_c)\beta}_{E_s} + \underbrace{f_c \left(\frac{W_c}{S}\right)^{1/2}}_{E_w} + \underbrace{B_c \left[1 - \left(\frac{W_c}{S}\right)^{1/2}\right]}_{E_t} \right\} E_p \quad (2)$$

where f_c is the canopy fraction, β is moisture availability constrained by the field capacity and wilting point of the soil, S is maximum W_c (constant), and B_c is the plant coefficient that includes the Jarvis (1976) stomatal resistance formulation. E_p is parameterized using the Penman–Monteith formulation with zero stomatal resistance.

2.1.3 VIC

The VIC model was developed in the early 1990's at the University of Washington. It is fundamentally different from CLM and Noah, as rainfall-runoff response is simulated using a variable infiltration curve that accounts for variations in landcover type at the sub-pixel level and baseflow is routed using a non-linear recession curve (Liang et al. 1994). The model has undergone a series of improvements, including the addition of a skin layer and parameterization of upward diffusion across soil layers (Liang et al. 1996b), inclusion of sub-grid variability in P (Liang et al. 1996a), a ground heat flux component that accounts for heat storage and diffusion across all soil layers and vegetation effects in the surface layer (Liang et al. 1999), a surface runoff component that accounts for infiltration excess (Liang and Xie 2001), and explicit representation of cold land processes (Cherkauer et al. 2003). The vegetation component consists of a single layer based on the atmosphere-canopy resistance formulation in Ducoudre et al. (1993). The formulation introduces an architectural resistance term that accounts for within-canopy effects on turbulent flux. VIC tends to underestimate soil moisture at mid-latitudes (Nijssen et al. 2001b) and overestimate Q in semi-arid regions (Nijssen et al. 2001a), which has been attributed to poor forcing data (precipitation) and over prediction of E_a .

The wet canopy and transpiration components of VIC are similar to Noah, as aerodynamic and canopy resistance including bulk limitations on soil moisture, temperature, and vapor pressure deficit are included in W_c .

Unlike Noah, S varies as a function of LAI. As with the other LSM's, E_p is defined using Penman–Monteith with zero stomatal resistance. The soil component of VIC employs an area integration to define the soil moisture constraint on E_p :

$$E_s[n] = \left\{ \int_0^A dA + \int_A^1 \frac{i_0}{i_m \left[1 - (1 - A)^{1/b}\right]} \right\} E_p \quad (3)$$

where E_s is the soil evaporation for landcover type n , A is the area of the soil profile, i_0 is the initial infiltration capacity, i_m is the maximum infiltration capacity, and b is a shape parameter for the infiltration curve. The first integral represents the saturated area which evaporates at the potential rate.

2.2 Hybrid models

The hybrid models were developed by combining the canopy component of a modified Priestley–Taylor model with the soil and wet canopy components of the Noah and VIC models by direct insertion. The vegetation component of the Fisher model is easily adapted for remote sensing and surface reanalysis data, including the introduction of an NDVI time series. This is particularly valuable in semi-arid areas, where NDVI climatology used by other LSM's does not adequately capture variability in E_a . A full description of the model, along with a bibliography highlighting major model advancements can be found in Fisher et al. (2008). The Fisher model has shown superior performance against other E_a models in the tropics, when compared using eddy covariance flux tower data (Fisher et al. 2009). Given uncertainties in the forcing data and parameterization of the wet canopy and soil evaporation components of the model, a hybrid was developed using the GLDAS 0.25° forcing data, Noah soil and wet canopy evaporation, and MODIS vegetation index products from 2000 to 2009 (Marshall et al. 2011). The hybrid model showed higher correlations and lower RMSE with observed data than the Noah or Fisher model. The hybrid, labeled Noah* in this paper, is parameterized instead with the 1.0° resolution GLDAS forcing data and Noah soil and wet canopy evaporation from 1979 to 2009. The vegetation indices were derived from version 3 of the Long Term Data Record (LTDR) (Nagol et al. 2009; Pedelty et al. 2007). The LTDR dataset consists of AVHRR daily reflectance at 0.05° resolution that has undergone rigorous inter-sensor calibration and atmospheric correction. The LTDR dataset ends in 2000, so the hybrid models were only run until then. The second hybrid model, labeled VIC*, combines the Fisher canopy component with the VIC wet canopy and soil evaporation components. The soil scheme and Q parameterizations in VIC, as briefly described above, tends to generate Q closer

to observed data than the soil scheme and Q parameterizations used in Noah and CLM (Wang et al. 2008).

2.3 Runoff data and model evaluation

The models were evaluated in a water balance approach using nine gauged stations representing major basins in Africa (Fig. 1). Monthly discharge data for these stations was acquired from the global runoff data centre (GRDC). The GRDC, directed by the World Meteorological Organization, compiles daily and monthly discharge data from stations across the globe. The monthly mean discharge data was converted to total annual runoff using catchment area from boundaries defined using the USGS EROS Hydro 1 K database derived from the GTOPO30 (1 km resolution) digital elevation model. Not all stations were located at the mouth of the watershed, so the upstream contributing area was determined using the Pfafstetter codes of each sub-basin and procedures described in Verdin and Verdin (1999). The Hydro 1 K boundaries compared well with a subset of boundaries determined using the 90 m resolution shuttle radar topography mission (SRTM) defined boundaries. Table 1 gives a brief summary of each station and upstream contributing area, including important eco-physiographic characteristics. With the exception of the Congo station, each station had at least 10 years of monthly data. The Nile station, which is a very small headwater catchment, was included to give a better representation of Q in tropical Africa. All of the catchment data ended in 2000, so the evaluation period spanned 1979–2000.

The stations were evaluated using a water balance approach. The difference between P and Q equals E_a at an annual time-step, assuming that soil moisture storage is negligible. This assumption is most appropriate for areas where the residence time of soil moisture is short (i.e. soils completely dry out between years) and where the change in soil moisture storage over time due to climate change/

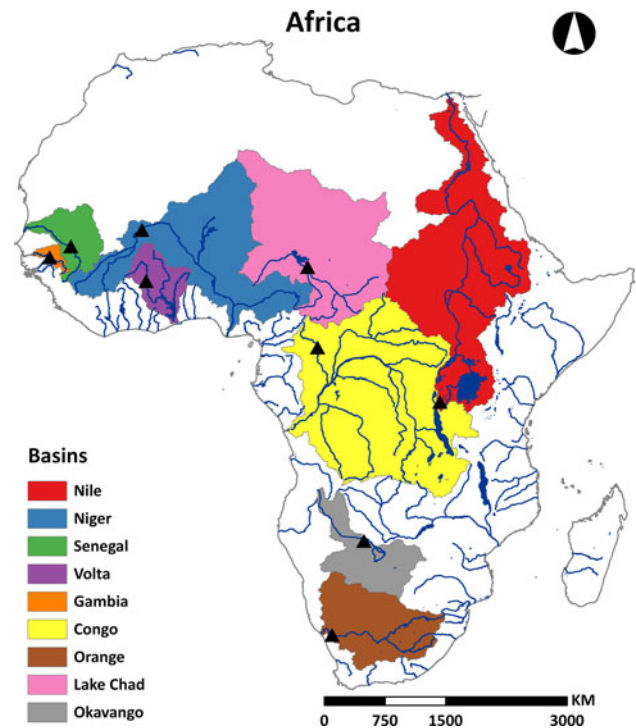


Fig. 1 Hydrologic stations measuring discharge from the upstream contributing area of nine major basins in sub-Saharan Africa. Monthly runoff from these stations were used with GLDAS precipitation in a water balance validation of E_a from three global land surface models and two model hybrids that are driven by a time series of remotely sensed vegetation indices

variability is close to zero. According to Milly et al. (2003), these areas fall primarily in the Sahel, Saharan Desert, and southern Africa, and exclude tropical Africa. The difference in annual total GLDAS P and observed Q derived from monthly means was plotted against modeled annual total E_a using a conventional time series plot and Taylor diagram. The Taylor diagram (Fig. 2a) summarizes the overall skill of a model by plotting the standard deviation on arcs that cross the x - and y -axis, the Pearson correlation

Table 1 The eco-physiographic characteristics of nine sub-basins used in the water balance evaluation of the E_a models

Basin	Sub-basin	GRDC	Period	Area (km ²)	Elevation (m)	IGBP	T (°C)	P (mm)	Q (m ³ /s)
Congo	Sangha	1,748,500	1985–1994	73,378	694	DBF	23.9	1,409	577
Gambia	Koulountou	1,813,320	1981–1995	6,802	110	OSH	27.6	901	27
Lake Chad	Chari	1,537,100	1982–1991	629,517	533	CSH/DBF	26.6	827	461
Niger	Dire	1,134,700	1981–1992	349,845	377	CSH/DBF/CRO	27.2	870	583
Nile	Kanyaru	1,670,200	1981–1991	5,156	1,630	CRO	19.4	1,054	23
Okavango	Mohembo	1,357,100	1981–2000	232,631	1,314	SAV	21.0	684	257
Orange	Vioolsdrif	1,159,100	1981–2000	510,828	1,293	SAV	16.6	483	150
Senegal	Kayes	1,112,100	1981–1990	125,027	371	OSH	27.6	788	224
Volta	Dapola	1,931,400	1981–1991	91,707	303	CRO	28.3	672	61

Each sub-basin includes a unique GRDC identifier. The dominant landcover type(s) for each sub-basin is shown using the International Geosphere-Biosphere Program (IGBP) naming convention

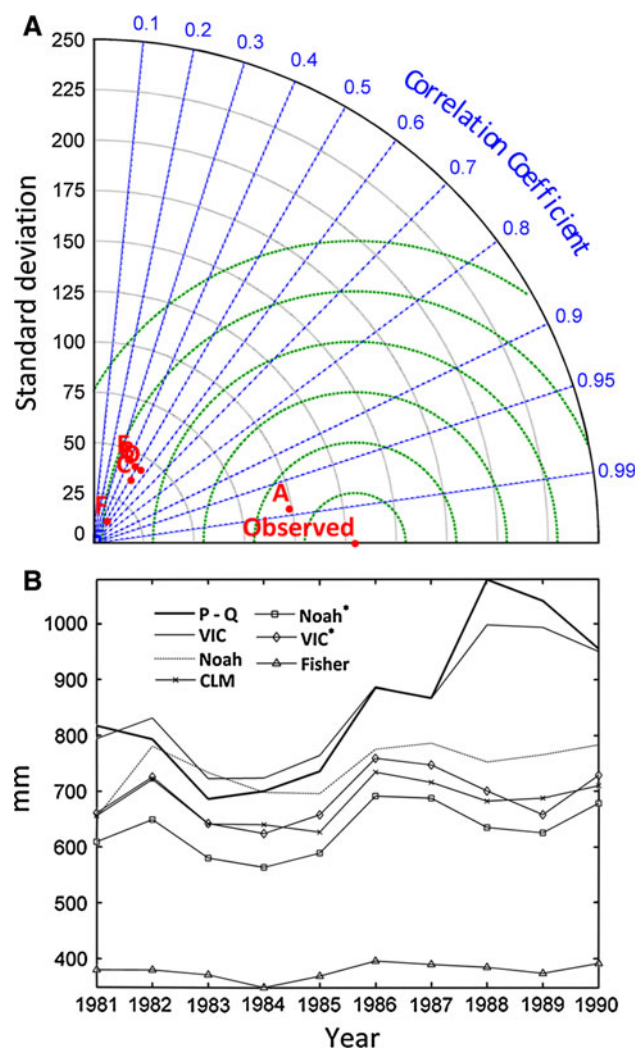


Fig. 2 Taylor diagram (a) and time series (b) of annual total P-observed runoff (Q) versus nine (A = VIC, B = Noah, C = CLM, D = Noah*, E = VIC*, and F = Fisher) E_a models for the Senegal basin. In the Taylor diagram, the correlation coefficient (shown on the primary arc) subtends arcs expressing STD (shown on the y axis). RMSD cross the STD arcs and are incremented at the same interval as STD. A model which accurately captures the structure, amplitude, and variability in observed annual E_a would fall on the point labeled “Observed”

(R) on the main arc, and the root mean square difference (RMSD) on the arcs that cross the standard deviation arcs (Taylor 2001). A model that reflects the timing and magnitude of observed E_a well will have a high R, low RMSD, and standard deviation close to the standard deviation of the observed data. Visually, this model will fall close to the point marked observed on the Taylor diagram.

2.4 Time series analysis

The time series analysis was performed on the E_a model that best reflected the timing and magnitude of observed Q

for the nine sub-basins on an annual basis. Linear and non-linear (Theil-Sen median slope) techniques at each grid cell of the image time series were used to determine the magnitude, direction, and significance of the trend. Trend analysis was performed on 31 years (1979–2009) of seasonal (December, January, February (DJF), March, April, May (MAM), June, July, August (JJA), and September, October, November (SON) totals for E_a and P and averages for minimum (T_{min}) and maximum (T_{max}) daily temperatures respectively. The 31 year time series at each grid cell was fit using linear regression and masked for 95% confidence (0.05 significance). The Theil-Sen method was selected as a complementary approach, because unlike linear techniques, the trends are not significantly impacted by outliers or missing data (Huth and Pokorná 2004). This is particularly important in this paper, where the trends are determined over several forcing datasets and the AVHRR data contains a large gap in 1994. Unlike non-parametric techniques, the magnitude and confidence intervals can be expressed for each trend using the Theil-Sen method. In the Theil-Sen method, the slope between each data pair of values in the time series is computed and the median value of the slopes is taken as the slope of the trend. Confidence intervals are expressed using the Mann-Kendall statistic. Standard linear regression at each grid cell was applied to the seasonal data to determine the strength and significance of the relationships between E_a , P, T_{min} , and T_{max} .

The trends in E_a timing at each grid cell were performed by applying the linear and Theil-Sen techniques to a harmonic regression at each grid cell of the image time series. In harmonic regression, a time series is fit by adding a series of sine and cosine functions or harmonics together (Wilks 1995). The harmonic regression was applied to monthly data on an annual basis. The first harmonic in this case represents peak E_a , which occurs during the primary growing season, while the second harmonic measures the second peak typically found during the secondary growing season in bimodal climate regimes. The equation for the first two harmonics is shown below.

$$y_t = y_0 + \sum_{k=1}^2 A_k \cos\left(\frac{2\pi kt}{n}\right) + B_k \sin\left(\frac{2\pi kt}{n}\right) \quad (4)$$

where y_t is the predicted variable (E_a) for year t, y_0 is the monthly mean value over year t, k is the frequency number, and n is the number of points in the series (n = 12). Higher harmonics would be appropriate for trimodal systems as can be found in the Ethiopian highlands (western Ethiopia), but these systems are rare and a risk is involved in over fitting the data. The trend analysis was therefore performed on the phase (timing) of the first two harmonics.

3 Results

3.1 Land surface model evaluation

The evaluation revealed on an annual basis that the VIC model performed equally as well or better than the other LSMs for all nine catchments in capturing the magnitude, timing, and variability of observed Q . The results of the original Fisher model were included as a baseline of comparison with the hybrid models. No observable trends were detected in the annual signal, as might be expected, assuming a change in water storage over time. CLM did well for many of the sub-basins, particularly for the only humid (tropical) sub-basin (Congo). The Fisher model showed significantly low correlations with Q for many of the sub-basins and greatly underestimated the variability in observed Q . Figure 2a, b show a Taylor diagram and time series of modeled E_a versus the difference of GLDAS P and observed Q for the Senegal sub-basin. Annual totals were derived

from monthly means. The RMSD on the Taylor diagram is incremented at the same interval as the standard deviation on the y -axis. The LSMs tend to correlate well with observed Q , but greatly underestimate the variability and show high RMSD. In the Senegal sub-basin, for example, the performance of the LSMs tends to diverge from VIC after 1985, missing the highest peak in 1988. The dissimilarity between the performance of the VIC model and the other LSMs is well represented for most of the sub-basins, as illustrated in Table 2. Given the relative magnitude of P over Q , the difference in P and E_a was plotted against observed Q , however there was no change in the outcome of the results. VIC does particularly well at the semi-arid sub-basins (Niger and Senegal), where the water balance assumption is most valid. It was expected that the hybrid models would perform better than VIC in these sub-basins, because they include a time series of vegetation indices. The hybrid models correlate better than VIC in the Congo sub-basin, but still underestimate the variability and show high RMSD.

Table 2 The correlation coefficient (R), standard deviation (STD), and root mean square difference (RMSD) of observed ($P-Q$) versus modeled AET for nine sub-basins in sub-Saharan Africa

Basin	Metric	VIC	Noah	CLM	Noah*	VIC*	Fisher
Congo (STD = 503.01)	R	0.96	0.96	0.98	0.98	0.98	0.94
	STD	474.69	411.94	403.88	381.24	378.17	220.26
	RMSD	141.36	162.48	131.15	151.21	151.31	303.59
Gambia (STD = 141.86)	R	0.87	0.64	0.84	0.78	0.74	0.57
	STD	130.64	99.59	83.04	86.75	83.92	56.83
	RMSD	70.96	109.61	84.76	92.01	97.91	118.72
Lake Chad (STD = 299.33)	R	0.98	0.94	0.97	0.95	0.94	0.85
	STD	285.84	267.85	230.59	222.82	231.12	186.43
	RMSD	31.45	68.43	83.76	94.99	90.07	189.10
Niger (STD = 106.72)	R	0.91	0.52	0.62	0.59	0.56	0.10
	STD	80.75	59.01	50.56	49.91	52.91	22.20
	RMSD	47.78	91.45	85.04	87.39	88.52	106.88
Nile (STD = 235.75)	R	0.98	0.94	0.97	0.95	0.94	0.85
	STD	162.56	156.25	138.96	137.13	125.44	108.74
	RMSD	83.04	102.25	105.75	114.41	126.28	154.08
Okavango (STD = 152.36)	R	0.97	0.88	0.93	0.82	0.71	0.12
	STD	155.48	119.29	111.95	105.67	117.87	152.93
	RMSD	36.91	73.09	64.40	89.45	106.95	202.92
Orange (STD = 202.26)	R	0.92	0.88	0.88	0.91	0.76	0.41
	STD	146.36	108.79	93.98	108.42	72.04	146.73
	RMSD	87.52	118.65	127.51	112.47	154.86	195.44
Senegal (STD = 129.67)	R	0.98	0.48	0.52	0.55	0.41	0.55
	STD	98.64	43.49	36.59	43.38	45.17	13.15
	RMSD	36.72	115.28	115.17	111.91	118.49	122.90
Volta (STD = 214.92)	R	0.99	0.94	0.94	0.93	0.93	0.92
	STD	216.82	181.00	177.41	171.18	186.24	96.70
	RMSD	15.35	75.38	76.09	85.21	78.01	132.30

The observed STD is indicated in parantheses

3.2 Seasonal trend analysis

The seasonal trend analysis revealed that steady declines in E_a over much of sub-Saharan Africa, coincide with increases in T_{max} and to a lesser extent P. The divergence E_a and P is most pronounced after the early 1990's and could be the result of temperature-moisture feedbacks in areas of high E_a variability (e.g. western Sahel) during the primary growing season (JJA). Figure 3 shows the results of the trend analysis for JJA. Grid cells with a value of zero showed no significant trend at the 95% CI. The sharp edges shown on this figure and related figures are a result of the confidence mask used and the spatial resolution of the surface reanalysis data. The trends in all figures were derived using the Theil-Sen method, as the linear trends and confidence mask were similar. Large E_a declines, on the order of 5 mm/year or 150 mm (nearly half of the seasonal average total) can be seen over much of coastal West Africa, the Sahel, and the Ethiopian highlands (western Ethiopia).

Figure 4 shows Pearson correlations between seasonal (JJA) total E_a and P and average daily T_{max} . The correlations

between T_{max} and P were determined from the residuals of each, given the strong relationship between E_a , T_{max} , and P across the region. This approach does not account for any covariance between T_{max} , E_a , and P. The correlations are significant at the 95% confidence band. Strong positive correlations (>0.6) between E_a and P can be seen over most of northern Africa. The strong correlations between E_a , T_{max} , and P do not show causality, but do reveal potential feedbacks which merit further analysis. For much of the areas showing declines in E_a , strong correlations between P and T_{max} exist. However, in these areas, T_{max} is increasing, while P remains unchanged. This is further elaborated upon in the following paragraph.

Figure 5 shows a scatterplot of JJA E_a and observed P and T_{max} for cropped areas in Senegal. Agriculture represents a significant and expanding portion of land use in the Sahel. The observed P shows a strong positive and significant relationship with E_a at the 99.9% CI. There is also a relatively weaker, but significant, negative relationship between T_{max} and E_a . This relationship is reflected in other cropped areas of the western Sahel where data was available

Fig. 3 The trend (per year) for JJA total evapotranspiration (E_a), total precipitation (P), minimum surface temperature (T_{min}), and maximum surface temperature (T_{max}). The trends have been masked for the 95% confidence band. Trends and confidence were computed using Sen's method of median slopes

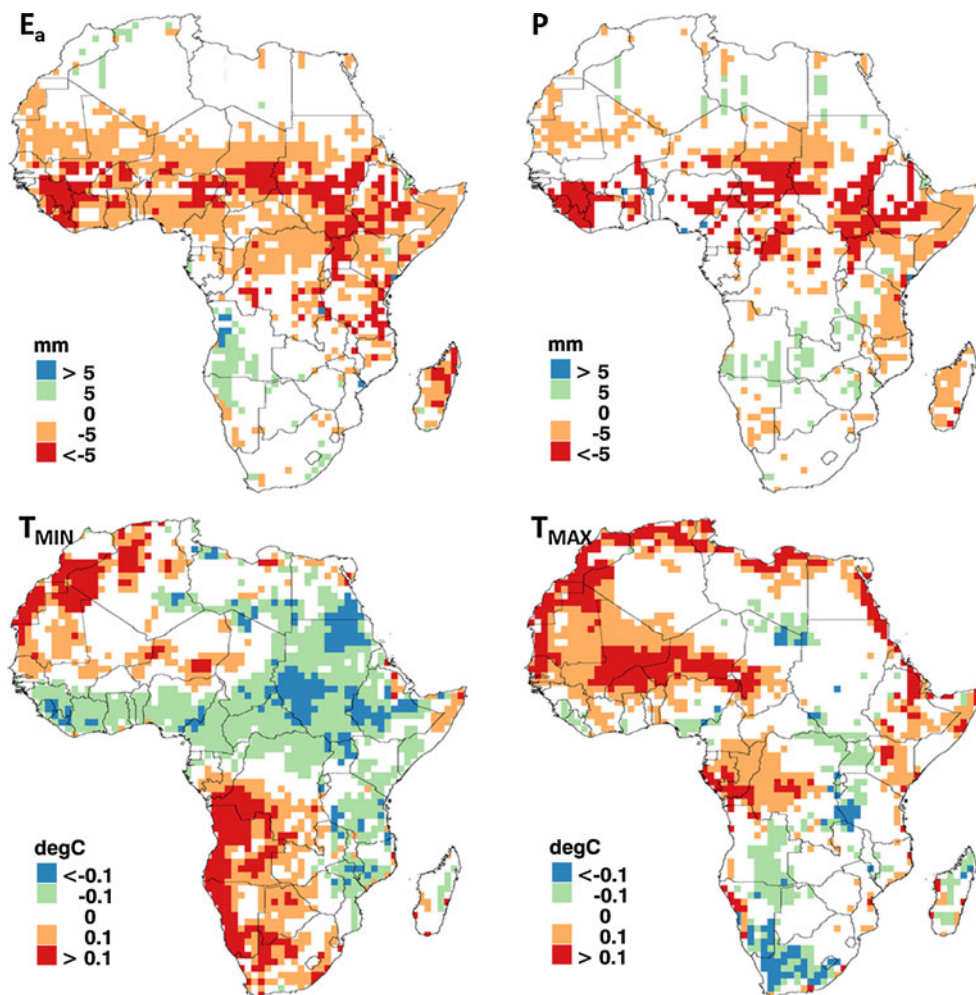


Fig. 4 The Pearson correlation (R) between seasonal total E_a and seasonal total P and seasonal average daily T_{max} for JJA. The correlations for T_{max} were determined from P and E_a residuals. Grid cells with a value of zero either showed no correlation or correlations that were not significant at the 95% confidence level

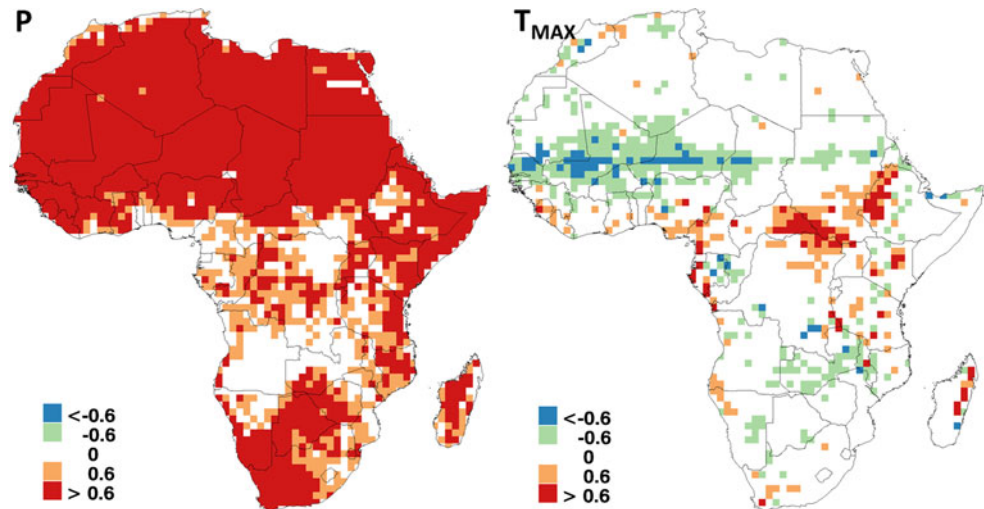
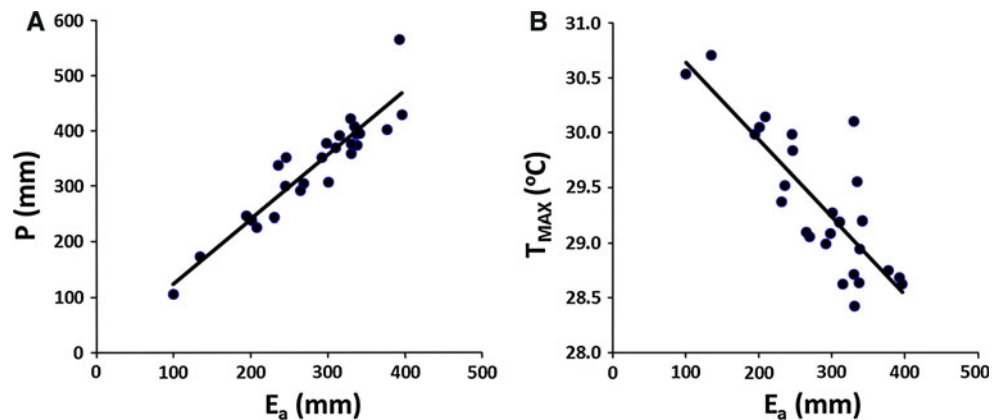


Fig. 5 JJA average E_a plotted against observed P (a) and T_{max} (b) masked for crop producing areas in Senegal. E_a declines correspond to increased T_{max} and an anti-correlation between T_{max} and E_a



(Burkina Faso $R^2 = 0.59, 0.88$; Mali $R^2 = 0.57, 0.78$; and Niger $R^2 = 0.74, 0.89$). A time series of the data (not shown) reveals after 1993, that a large increase in T_{max} corresponds to a recovery in P declines from the previous decade and continued declines in E_a . The potential decoupling of E_a and P could be the result of agricultural expansion. In southern Sudan and the Ethiopian highlands the temperature- E_a relationship is reversed. The positive relationship between T_{max} and E_a appears to fall outside areas with a strong moisture relationship, so vegetation may be less constrained by moisture: increases in daytime temperatures and E_p lead to increases in E_a . Southern Sudan reflects this pattern, as declines in T_{max} correspond to declines in E_a . The simulated declines in T_{max} , however, do not agree with observed data, which showed dramatic increases in T_{max} in this region. No significant change in T_{max} or E_a was detected in the Ethiopian highlands where the temperature relationship exists.

Figure 6 shows the average soil moisture (depth = 0–10 cm) for December, January, February (DJF); March, April, May (MAM); June, July, August (JJA); and September, October, November (SON). The soil moisture in the top layer tends to track the progression of Intertropical

Convergence Zone (ITCZ), with the lowest and highest soil moisture storage occurring over the Sahel during DJF and JJA respectively. The high positive correlation between E_a and P and relatively low soil storage over most of North Africa indicates that water input in this region is primarily evaporated away. The steady declines in E_a and P over coastal West Africa and the eastern Sahel (southern Chad and Sudan) and results from previous work (e.g. Douville 2002) suggest that these declines are amplified by a strong E_a and P positive feedback. Decreases in T_{min} or dew point temperature and relative humidity would favor increased subsidence, which further corroborates declines in precipitation, but correlations between T_{min} and E_a in this region are low. There is a strong negative correlation in the western Sahel and positive correlation in the eastern Sahel and Ethiopian highlands between T_{max} and E_a . The strong negative relationship between T_{max} and E_a in western Sahel and declining trends in E_a suggest a relationship between the two. If there is sufficient moisture in the root zone to maintain plant functions, plants will continue to transpire as daytime temperatures increase atmospheric demand (E_p) (Buckley 2005). According to Morton (1983), if soil

moisture is low in the root zone, as indicated by Fig. 6, E_a (latent heat) will decrease, leading to an increase in sensible heating, surface temperatures, and atmospheric demand. Given that there was no trend detected in P , we suggest that lower E_a may be contributing to increases in surface temperatures. This contribution has likely combined with sensible heat advection from surrounding areas and direct radiative forcing from greenhouse gasses and aerosols. While more research into the relative components seems warranted, the role played by the sensible/latent heating partitioning appears likely to play an important and perhaps unexpected role.

Land use and cover change could in combination with regional climatic drivers also affect E_a trends. The conversion of native vegetation to croplands for example, would reduce evapotranspiration (Zeng 2003), increase sensible heating (T_{max}), and increase the absorption of light for crop production, favoring a higher NDVI (Herrmann et al. 2005). Figure 7 represents the change in land cover from natural vegetation to croplands in Sahelian countries between 2005 and 2009. Two maps of annual land cover (2005 and 2009) distributed as part of the European Space

Agency (ESA) GlobCover project were used to develop the change map. The maps are derived from 300 meter spatial resolution MERIS (Medium Resolution Imaging Spectrometer) surface reflectance mosaics. The mosaics undergo rigorous geolocation and atmospheric correction before a combination of supervised and unsupervised spectral classifiers that account for regional characteristics are used to define 22 unique land cover classes (Bontemps et al. 2010). The maps are validated using hundreds of ground control points across the globe. Land cover classified as irrigated crops, rain-fed crops, and mixed cropland and natural vegetation (primarily grasslands and shrublands) were combined to define the extent of cropped area. The change map reveals that significant portions of native vegetation have been converted to croplands in the area corresponding to increases in T_{max} and declines in E_a between 2005 and 2009. Although many of these changes over such a short time frame could be the result of crop rotation or response to climate variability, the average increase across Sahelian countries is 14.25%, with more staggering increases in countries such as Mali (24.6%) and Mauritania (38.63%), suggesting that some of this change is permanent. VIC

Fig. 6 Seasonal soil moisture for top (0–10 cm) soil layer as modeled using VIC. Seasons are defined as (DJF—December, January, February), (MAM—March, April, May), (JJA—June, July, August), and (SON—September, October, November)

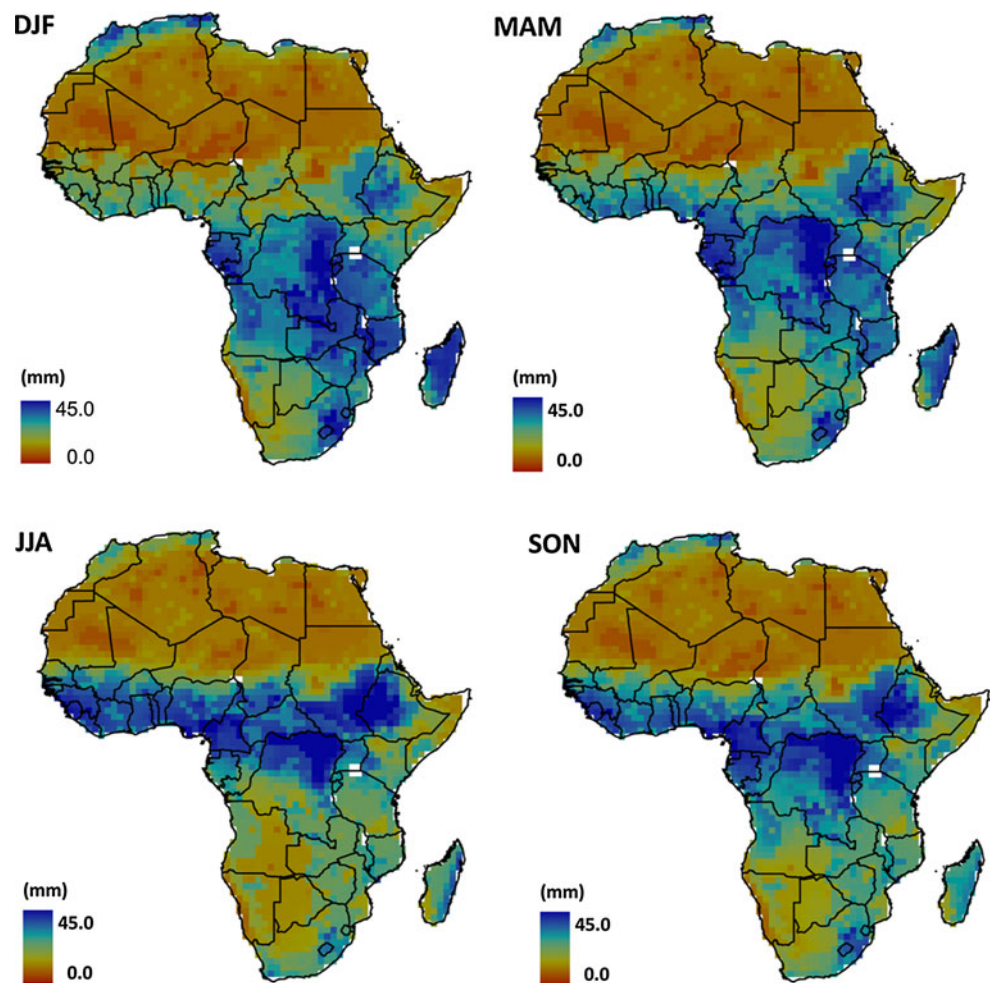


Fig. 7 Land cover change between 2005 and 2009 for the Sahelian countries (Burkina Faso, Chad, Eritrea, Ethiopia, Mali, Mauritania, Niger, Nigeria, Senegal, and Sudan) using the ESA GlobCover data product. Areas in yellow and turquoise show baseline (2005) cropland and predominantly native vegetation respectively, while areas in red show new cropland areas as of 2009

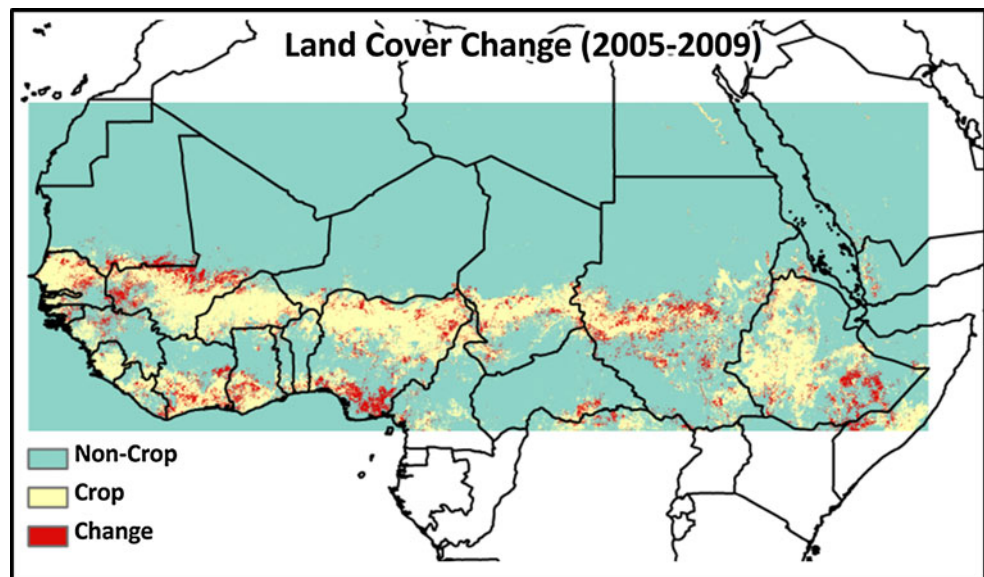
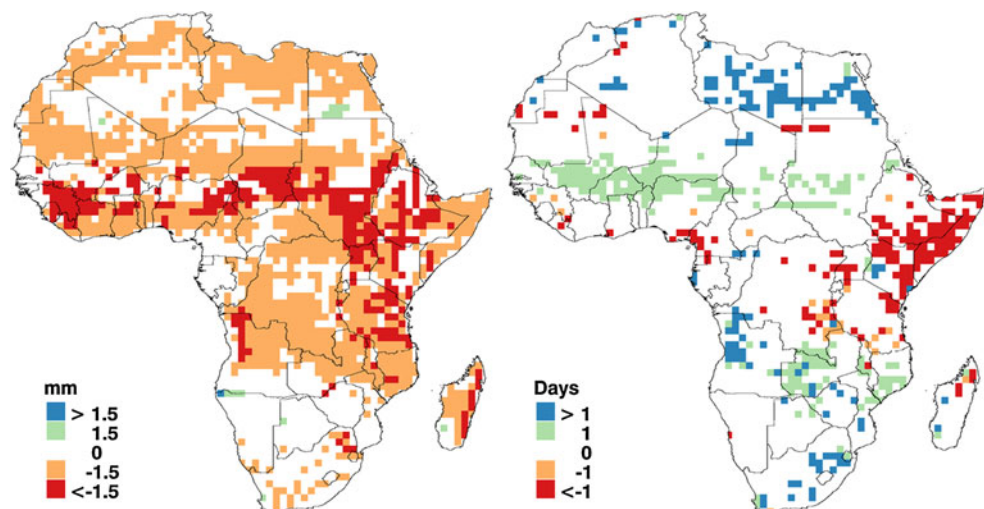


Fig. 8 The trend in the phase of E_a expressed in days for the first harmonic (primary growing season) of the harmonic regression at each grid cell. Grid cells with a value of zero either showed no correlation or correlations that were not significant at the 95% confidence level



incorporates land use and cover, but not change. The hybrid models include a dynamic vegetation component which captures this change, but did not perform as well as the original VIC, revealing that land use and land cover change may not play either a significant role in surface moisture flux dynamics or at the very least, in controlling E_a in the context of the VIC model. Further analysis, particularly at the catchment scale using field data appears warranted.

Similar trend analyses were performed for the other seasons, but the extent and correlation between E_a and climate change drivers were not as significant as in JJA. One notable exception was E_a declines corresponding to P declines over central Kenya, Tanzania, Uganda, northern Mozambique, and southern Ethiopia during the primary growing season (MAM). Figure 8 shows the change in amplitude and phase of peak E_a , which corresponds to the critical reproductive (“grain filling”) phase of plant

development. The trends are expressed in days and represent the change in amplitude and phase of E_a from the first harmonic of the harmonic fit. The trend analysis from the second harmonic (not shown) was highly sporadic, revealing only localized changes in the secondary growing season. In the western Sahel, peak E_a from the primary growing season has advanced by nearly 1 day per year (or 1 month over the 31 year time series). In the Horn of Africa (Kenya, Ethiopia, and Somalia), peak E_a from the primary growing season appears to be occurring 1 month or earlier in the year.

4 Discussion

This paper characterizes changes in E_a on a regional basis in sub-Saharan Africa using remote sensing and surface reanalysis data. The results of the Theil-Sen and linear

methods were very similar, reflecting the overall robustness of the results. The results agree with previous studies (see Dai 2010 for a review) that show a general drying over much of Africa and the divergence in the continental water cycle attributed primarily to the E_a response to decreases in P and soil moisture supply. These trends as reflected by ground-based and bias corrected satellite data appear to diverge from IPCC projections, which expect moderate increases in precipitation over this century (Brown and Funk 2008). In this paper, we add, based on the 31 year time series analysis of modeled data that E_a and P are becoming decoupled in areas where a strong relationship between the two have been observed, while temperature continues to increase. This relationship is most prevalent during the primary growing season in the northern hemisphere of Africa (JJA). In the western Sahel, an inverse relationship between T_{\max} and E_a and direct relationship between P and E_a were observed. Since no significant decreasing trend in P was observed in the region, the simulated data suggests that significant declines in E_a and latent heat are increasing sensible heat and surface air temperatures. In this semi-arid region, soil moisture storage is low, so it is expected that atmospheric demand is increasing in response to decreases in E_a according to Morton's hypothesis. Although the VIC model does not include a stomatal resistance component, LSMs that do, reflect similar patterns between E_a and T_{\max} attributed to plant response to increased moisture stress.

After 1993, P declines in the Sahel appear to be rebounding, while E_a declines continue. While 1993 denotes a transition period for the forcing data, the recovery in Sahelian rainfall has been documented in previous studies using observed and other simulated data (Funk et al. 2011; Hoerling et al. 2009; Lebel and Ali 2009). Given the historic coupling between rainfall increases and temperature decreases in the Sahel, the recent increases in temperatures, which have been validated through analyses of station measurements (Funk et al. 2011) are quite striking, and the decline in E_a corresponds to a dramatic increase in daytime temperatures after 1993. The decline in E_a and latent heat and rise in sensible heating and T_{\max} could result in a positive feedback between E_a and T_{\max} , which could lead to further divergence in the water balance. The decoupling of P and E_a is occurring in areas where daily maximum temperatures exceed 40°C throughout much of the year. At high temperatures, the relationship between T_{\max} and the saturation vapor pressure becomes exponential, so small increases in temperature could produce significant increases in atmospheric demand, further limiting healthy plant function and consequently enhancing desertification. The impact of the temperature-moisture relationship on plant health in the western Sahel and Africa has been explored in previous

studies using NDVI (Brown and de Beurs 2008; Vrieling et al. 2011) with results similar to this study. The results could be further explored and refined using a crop model or MODIS land surface temperature (LST) which is likely closer to plant temperature than air temperature. The introduction of observed energy and moisture flux data via the African Monsoon Multidisciplinary Analyses (AMMA: <http://amma-international.org/>) should improve the understanding of the temperature-moisture relationship as well.

Landcover change and other non-climatic related factors could be affecting the simulated temperature-moisture relationships as well. The steady decline in E_a over the western Sahel coincides with a steady increase in photosynthetic activity, as shown using NDVI (Herrmann et al. 2005; Heumann et al. 2007; Vrieling et al. 2011) and land cover maps in this study. The apparent discrepancy between E_a declines and increasing NDVI, suggests that natural (perennial) vegetation is being converted to annual crops. Natural vegetation tends to have greater access to soil moisture than annual crops, because it has a deeper root zone. Natural vegetation therefore tends to have higher seasonal total E_a than annual crops. Annual crops produce more biomass than natural vegetation, so NDVI tends to be higher for the former, even though annual E_a is lower than the latter. The harmonic regression analysis revealed a later green-up in this area, suggesting that annual crops, which tend to green-up earlier than natural vegetation, contradicts this hypothesis. The NDVI time series used in temporal studies in the Sahel are derived from global inventory modeling and mapping studies (GIMMS) Group at NASA's Goddard Space Flight Center (Tucker et al. 2005). The GIMMS dataset is problematic for time series analysis, because inter-calibration errors and orbital drift can affect sun-sensor geometry and the magnitude of the vegetation index across the multiple AVHRR sensors used to develop the series (Nagol et al. 2009). So, if the observed positive NDVI trend in previous studies is false, desertification could also lead to a negative T_{\max} and E_a relationship. If NDVI were declining due to desertification, the reduction in plant biomass and E_a would lead to higher sensible heating and increase T_{\max} . Observed higher water tables in Niger and other parts of the Sahel would support either of these hypotheses, as desertification and lower ground cover would enhance Q , while the conversion of natural vegetation with roots adapted to access relatively deep ground water to croplands with shallow roots would lead to an increase in Q (Boone 2011). The influence of landcover on potential temperature-moisture feedbacks is unresolved and appears to be an important area for further study.

The largest simulated declines in E_a are in coastal West Africa. This area has relatively higher soil moisture storage and E_a shows strong correlations with P and weak

correlations with temperature, so we expect that E_a declines are driven primarily by declines in soil moisture supply. Unlike the Sahel and Ethiopian highlands, which showed gradual declines in E_a over the 31 year time series, the trend in coastal West Africa appears to be driven primarily by precipitation fluctuations associated with decadal variations in sea surface temperatures (SST). This concurs with Lebel and Ali (2009) who showed continued declines in P in coastal West Africa, while the western Sahel showed rainfall recovery in the early 1990's. Due to its proximity to the ocean, declines in P and E_a in coastal West Africa in the 1980's coincide with decreased warming in the northern tropical Atlantic Ocean and increased warming in the Indian Ocean. Cooling in the northern tropical Atlantic occurs when the northern migration of the ITCZ (tropical convection) contracts at the onset of the Atlantic Monsoon (Chiang and Vimont 2004). The cooling creates a region of stability and drying which prevents moisture transport into coastal West Africa (Hagos and Cook 2008). Warming in the Indian Ocean creates an area of deep convection which draws moisture from and forces subsidence in this region as well. E_a increases in the early 1990's are followed by a brief period when warming in the northern tropical Atlantic appears to have increased convection and moisture flux onto the continent. Temperatures in the northern tropical Atlantic since the early 1990's have remained above normal, though declines in E_a reappear and are intensified. Warming in the Indian Ocean continues and has intensified since the early 1990's and the E_a declines could be reflecting the prominence of Indian Ocean SSTs in driving P in this region. The role of SST's and general circulation in impacting P has been studied in this region extensively (e.g. Biasutti et al. 2008), however the full land–ocean feedback, which includes the regional influence of E_a should be explored in the future.

Declining trends in E_a and its relation to climate drivers in the Eastern Sahel and the Horn of Africa are less clear, particularly for surface temperature, and should be revisited, assuming Indian Ocean SST warming continues and its impact in these areas intensifies. The decrease in E_a over central Kenya, Tanzania, Uganda, and southern Ethiopia in MAM and Sudan and Ethiopia in JJA and their correlation with P reflects a general drying pattern that has been attributed using climate reanalysis (Minobe 2005) and observed data (Williams and Funk 2010) to warming in the Indian Ocean. As in West Africa, the warming draws moisture from and induces subsidence over Eastern Africa. Subsidence over most of Eastern Africa is reflected by decreases in P and T_{min} (an indicator of dew point), though no strong relationship was simulated between T_{min} and E_a . Subsidence and increased low-level stratus cloud cover could also explain the decrease in T_{max} for a narrow corridor in southern Sudan in JJA, however the observed data did not agree with these declines. It

is unclear why the simulated temperature data did not agree with observed data in this area, but dramatic changes in topography or the lack of station data to remove bias in the reanalysis data could be the cause. It should also be noted that large increases in T_{max} were observed during MAM over much of the Sahel. The causal link between E_a and T_{max} is difficult to discern, as these trends occurred outside the primary growing season (JJA). One possibility could be that vegetation in Sudan often increases productivity before the rainy season in order to have a full canopy that provides shade and conserves moisture during the rainy season (De Bie et al. 1998). Increased temperatures before the rainy season could therefore put moisture stress on vegetation that leads to lower productivity during the primary growing season. More localized studies that employ higher spatial resolution datasets that account for fine scale variability in landcover and topography and expand on the understanding of vegetation response to increased subsidence may resolve the temperature–moisture feedbacks simulated in the Sahel.

The large decline in E_a over much of northern Africa during the primary growing season and throughout the year in rainforests in the Ivory Coast, Liberia, Sierra Leone, Congo basin, and Eastern Madagascar has major ramifications for ecosystem health and development. The declines in E_a could be a result of deforestation. The Ivory Coast, Liberia and Sierra Leone have lost between 60 and 85% of their forests already, while deforestation in the Congo basin is becoming a growing concern (FAO 2010). Rainforests are a major source of moisture flux, are critical to global carbon cycling, and harbor a high level of biodiversity. Quantifying deforestation at the global level remains an active area of research. E_a modeling could help to improve these mapping efforts. Natural landcover in the Sahel and Ethiopian highlands consist primarily of grasslands, savanna, shrublands, and woodlands, while land-use consists primarily of rain-fed subsistence cultivation and grazing. The large and significant decrease in E_a in these regions, indicative of over-cultivation and/or desertification, will undoubtedly further endanger natural ecosystems, as growing population demands in these fringe areas will increase the need for grazing and farm land.

The trends in the timing of E_a are also alarming, because a change in timing could jeopardize ecosystem productivity. In addition, agriculturists and pastoralists in these areas depend on regular timing of plant development in order to maximize crop productivity. In the Horn of Africa, the 1 month or earlier trend in peak E_a corresponds to declines in P . Given the relatively low soil moisture storage during the peak season (JJA), natural vegetation may be assimilating carbon or farmers may be planting earlier in the season, in order to maximize early moisture withdrawals. The month delay in peak E_a that was shown over the western Sahel complements previous studies using NDVI

(see Heumann et al. 2007). Unlike the Horn of Africa, the Sahel shows a strong temperature– E_a and weak P – E_a relationship. The rise in temperature and increase in sensible heating could result in a delayed “green-up.” Annual crops in the Sahel can lay dormant, if rainfall is insufficient. Since the rainfall trends are insignificant in this region, it is possible that increased temperature may lead to delayed germination brought on by increased E_p . Although this paper looks at E_a phase, we did not partition the trend into its constituent parts (start of season, end of season, and length of growing season). Further study on how these feedbacks affect each major component of plant phenology could help to resolve these hypotheses.

The results of this paper should be regarded with care, as the trend analysis was performed on model estimates driven by various remote sensing and climate surface reanalysis datasets. In addition, the observation data used to validate the VIC model did not cover the entire 31 year time series. This is critical, since many of the more sophisticated remote sensing and observation based datasets were not integrated into GLDAS until after the validation period. Although the datasets have been synthesized, it is difficult to know if the more dramatic trends in E_a after the 1990's are due to cloud forcing common in satellite born data. Observed P and T_{max} , for example, corroborate the P and T_{max} trend results in the western Sahel, but not simulated T_{max} trends in southern Sudan. The Noah hybrid model was evaluated using eddy covariance flux tower data after 2000 in Marshall et al. (2011), so one might assume that VIC would do better in the modern era as well, but that paper used higher spatial resolution forcing data and better vegetation (MODIS) data, so future work should aim to evaluate the LSMs using more modern observation data.

The evaluation dataset may give misleading results as well. Modeled E_a and observed Q were much lower than GLDAS P , particularly for the semi-arid sub-basins. VIC model performance therefore may be superior at the semi-arid sub-basins, because P – Q response is stronger than the other models. In this respect, the performance of the Fisher E_a could be obscured, because it is not coupled to GLDAS P . The superiority of the VIC model for the semi-arid catchments could be due to other factors as well. The VIC model includes the most sophisticated soil evaporation component and is strongly coupled to precipitation. The coupling of soil moisture and precipitation is particularly strong along the Sahel, particularly after a rain event. Another possibility is that the VIC model, which requires stream flow data to calibrate the infiltration curve, could have been calibrated using the same stream flow data. The poor performance of the Fisher model in semi-arid regions has been attributed to poor soil parameterization and reanalysis surface specific humidity and pressure (see Marshall et al. 2011). The VIC and NOAH models, which are strongly coupled to precipitation and not specific humidity,

reinforce the superiority of the VIC soil component in capturing the timing and magnitude of Q in semi-arid regions. One possible solution to resolve these issues would be to evaluate the models using an independent P source, but the difficulty in separating E_a performance from P performance remains.

The assumption that soil moisture storage is negligible at an annual time step is most appropriate for semi-arid sub-basins where the most striking trends were simulated. No significant trends in soil moisture were simulated over the Sahel, as is expected, because these basins tend to dry out between years and the simulated change in soil moisture storage over time is close to zero. In the Congo Basin, however declining trends have been simulated in previous studies, but the magnitude and significance of this change is under debate (see Llovel et al. 2010). Trend detection in the Congo Basin is difficult, due to its proximity to two oceans. As a result, the basin exhibits a “seesaw” climate, so trends could be capturing actual change or variability. Assuming that the declining trends in the basin are real, the underestimation of the models should be considered grossly underestimating to accommodate the anticipated decline in Q . A critical evaluation of regional ground water storage and its impacts on E_a and atmospheric feedbacks should be performed in future studies.

The performances of the model hybrids and CLM at first seem counterintuitive, because the use of a canopy component driven by a time series of vegetation indices in the case of the hybrids and the use of a sophisticated stomatal resistance component should capture the variability better at drier sites. Like the Fisher model, CLM is not as strongly coupled to precipitation as NOAH or VIC and this might have some influence on its poor performance for drier catchments. Rosero et al. (2009) showed that vegetation index time series improve the canopy component of E_a at humid sites and not drier sites. This could be due to inherent multi-sensor errors with the AVHRR data as discussed above and the dominance of bare soil at drier sites that could be obscuring the vegetation signal in coarse spatial resolution datasets. The lack of an advection term in the Priestley–Taylor formulation for E_p could also be a factor in the case of the Fisher model, as advection tends to be an important component of E_p in dry regions, however the substitution of the Priestley–Taylor formulation for E_p with one that includes an advection term did not improve the results of that analysis. These data issues should be addressed as the process of model improvement continues.

5 Conclusion

This paper uses remote sensing and surface climate reanalysis data to identify important temperature and moisture relationships with evapotranspiration. In the

western Sahel, a potential positive daytime temperature and evapotranspiration feedback exists: decreased evapotranspiration and latent heating is leading to increased sensible heating and daytime temperature which increases atmospheric demand and further decreases evapotranspiration. The African continent is expected to experience an annual 3–4°C increase in surface temperatures by the end of the 21st century, according to the IPCC A1B ensemble mean (Christensen et al. 2007). The IPCC projects that temperatures in subtropical regions (particularly the Saharan desert and Sahel) will warm more than the humid tropics. This feedback would therefore likely intensify under projected IPCC projected climate warming. The increase in sensible heating, resulting from this warming will likely delay the reproductive phase of the growing season, which will further strain natural ecosystems, farmers, and pastoralists who depend on regular timing of plant phenology. Projected changes in precipitation in the Sahel are less known, given systematic errors in global simulations, lack of RCM simulations, and uncertainties in empirically derived downscaling techniques. The most plausible scenario suggested by the IPCC is that lower pressure (convergence) over the Sahel during JJA will bring modest increases in precipitation (~5%) by the end of the 21st century. The simulated historical trends from this study suggest, however, that the Sahel will get drier. This could be due to other mechanisms related to global warming, such as moisture divergence over the Sahel driven by warming in the Indian Ocean. Given the strong dependence of evapotranspiration on soil moisture, it is likely that under a “drier” scenario that declining trends in evapotranspiration in the Sahel will continue. El Nino events are characterized by elevated SST due to the equatorward migration of the ITCZ. This results in a strengthening of the Hadley Cell circulation and weakening of the Walker Cell circulation, which produces above normal rainfall in east Africa and drought conditions in southern Africa. Rainfall projections in east and southern Africa indicate that these areas will likely become more El Nino like by the end of the 21st century. The simulated data suggests, however, that Ethiopia, Somalia, Kenya, and northern Uganda are becoming drier and given the dependence of evapotranspiration on soil moisture in this area, desertification is likely to increase. Many articles related to ecological change have identified southern Africa as a 21st century hotspot, given the El Nino like climate projections. This study suggests, however, that the Sahel is showing larger and more significant declines in precipitation, which will be exacerbated by warming and potential temperature feedbacks. If this scenario continues, the Sahel will see larger and significant declines in evapotranspiration. Dramatic shifts in moisture flux in this region will have important ecological ramifications for sub-Saharan Africa and northern latitudes, making this a global concern.

References

- Allen CD et al (2010) A global overview of drought and heat-induced tree mortality reveals emerging climate change risks for forests. *For Ecol Manag* 259:660–684
- Anyamba A, Eastman JR (1996) Interannual variability of NDVI over Africa and its relation to El Nino/Southern Oscillation. *Int J Remote Sens* 17:2533–2548
- Berg AA et al (2003) Impact of bias correction to reanalysis products on simulations of North American soil moisture and hydrological fluxes. *J Geophys Res* 108:4490
- Betts AK et al (1997) Assessment of the land surface and boundary layer models in two operational versions of the NCEP Eta model using FIFE data. *Mon Weather Rev* 125:2896–2916
- Biasutti M et al (2008) SST forcings and Sahel rainfall variability in simulations of the twentieth and twenty-first centuries. *J Clim* 21:3471–3486
- Bonan GB (1996) A land surface model (LSM version 1.0) for ecological, hydrological, and atmospheric studies: technical description and user's guide. NCAR, Boulder, CO
- Bonan GB (1998) The land surface climatology of the NCAR land surface model coupled to the NCAR community climate model. *J Clim* 11:1307–1326
- Bontemps S et al (2010) GlobCover 2009: products description and validation report. Université catholique de Louvain, Louvain-la-Neuve, Belgium
- Boone A (2011) Land cover influences on temperature, precipitation, and evapotranspiration in the Sahel. In: Marshall M (ed) (personal communication), Santa Barbara, CA
- Brown ME, de Beurs KM (2008) Evaluation of multi-sensor semi-arid crop season parameters based on NDVI and rainfall. *Remote Sens Environ* 112:2261–2271
- Brown ME, Funk C (2008) Food security under climate change. *Science* 319:580–581
- Buckley TN (2005) The control of stomata by water balance. *New Phytol* 168:275–292
- Camberlin P et al (2007) Determinants of the interannual relationships between remote sensed photosynthetic activity and rainfall in tropical Africa. *Remote Sens Environ* 106:199–216
- Chen F et al (1996) Modeling of land surface evaporation by four schemes and comparison with FIFE observations. *J Geophys Res* 101:2896–2916
- Chen F et al (1997) Impact of atmospheric surface-layer parameterizations in the new land-surface scheme of the NCEP mesoscale Eta model. *Boundary Layer Meteorol* 85:391–421
- Cherkauer KA et al (2003) Variable infiltration capacity cold land process model updates. *Global Planet Change* 38:151–159
- Chiang JCH, Vimont DJ (2004) Analogous Pacific and Atlantic Meridional Modes of tropical atmosphere-ocean variability. *J Clim* 17:4143–4158
- Christensen JH et al (2007) Regional climate projections. In: Solomon S et al (eds) *Climate change 2007: the physical science basis/contribution of working group I to the fourth assessment report of the intergovernmental panel on climate change*. Cambridge University Press, Cambridge, New York, NY, pp 847–940
- Cook BI et al (2006) Soil moisture feedbacks to precipitation in Southern Africa. *J Clim* 19:4198–4206
- Dai A (2010) Drought under global warming: a review. *Wiley Interdiscip Rev Clim Change*. doi:10.1002/wcc.1081
- Dai Y, Zeng Q (1997) A land surface model (IAP94) for climate studies part I: formulation and validation in off-line experiments. *Adv Atmos Sci* 14:433–460
- Dai Y et al (2003) The common land model. *Bull Am Meteorol Soc* 84:1013–1023

- De Bie S et al (1998) Woody plant phenology in the West Africa savanna. *J Biogeogr* 25:883–900
- DehghaniSanij H et al (2004) Assessment of evapotranspiration estimation models for use in semi-arid environments. *Agric Water Manage* 64:91–106
- Derber JC et al (1991) The new global operational analysis system at the national meteorological center. *Weather Forecast* 6:538–547
- Dickenson RE et al (1986) Biosphere-atmosphere transfer scheme (BATS) for the NCAR community climate model. National Center for Atmospheric Research, Boulder
- Dickinson RE et al (2006) The community land model and its climate statistics as a component of the community climate system model. *J Clim* 19:2302–2324
- Douville H (2002) Influence of soil moisture on the Asian and African monsoons. Part II: interannual variability. *J Clim* 15:701–720
- Ducoudre NI et al (1993) SECHIBA, a new set of parameterizations of the hydrologic exchanges at the land-atmosphere interface within the LMD atmospheric general circulation model. *J Clim* 6:248–273
- Ek MB et al (2003) Implementation of Noah land surface model advances in the National Centers for Environmental Prediction operational mesoscale Eta model. *J Geophys Res* 108:8851
- FAO (2010) Global forest resources assessment 2010: main report. Rome, Italy
- Fischer EM et al (2007) Soil moisture-atmosphere interactions during the 2003 European summer heat wave. *J Clim* 20:5081–5099
- Fisher JB et al (2008) Global estimates of the land-atmosphere water flux based on monthly AVHRR and ISLSCP-II data, validated at 16 FLUXNET sites. *Remote Sens Environ* 112:901–919
- Fisher JB et al (2009) The land-atmosphere water flux in the tropics. *Glob Change Biol* 15:2694–2714
- Funk C, Michaelsen J, Marshall M (2011) Mapping recent decadal climate variations in Eastern Africa and the Sahel. In: Anderson M, Verdin J (eds) Remote sensing of drought: innovative monitoring approaches. Taylor and Francis, London, p 270
- Giannini A et al (2003) Oceanic forcing of sahel rainfall on interannual to interdecadal time scales. *Science* 302:1027–1030
- Giannini A et al (2008) A climate model-based review of drought in the Sahel: desertification, the re-greening and climate change. *Global Planet Change* 64:119–128
- Hagos SM, Cook KH (2008) Ocean warming and late-twentieth-century sahel drought and recovery. *J Clim* 21:3797–3814
- Herrmann SM et al (2005) Recent trends in vegetation dynamics in the African Sahel and their relationship to climate. *Glob Environ Change Part A* 15:394–404
- Heumann BW et al (2007) AVHRR derived phenological change in the Sahel and Soudan, Africa, 1982–2005. *Remote Sens Environ* 108:385–392
- Hoerling M et al (2009) Regional precipitation trends: distinguishing natural variability from anthropogenic forcing. *J Clim* 23:2131–2145
- Hogue TS et al (2005) Evaluation and transferability of the Noah land surface model in semiarid environments. *J Hydrometeorol* 6:68–84
- Huntington TG (2006) Evidence for intensification of the global water cycle: review and synthesis. *J Hydrol* 319:83–95
- Huth R, Pokorná L (2004) Parametric versus non-parametric estimates of climatic trends. *Theor Appl Climatol* 77:107–112
- Idso SB (1981) A set of equations for full spectrum and 8- to 14 micrometer and 10.5- to 12.5 micrometer thermal radiation from cloudless skies. *Water Resour Res* 17:295–304
- Jacquemin B, Noilhan J (1990) Sensitivity study and validation of a land surface parameterization using the HAPEX-MOBILHY data set. *Boundary Layer Meteorol* 52:93–134
- Jarvis PG (1976) The interpretation of the variations in leaf water potential and stomatal conductance found in canopies in the field. *Philos Trans R Soc B-Biol Sci* 273:593–610
- Jung M et al (2010) Recent decline in the global land evapotranspiration trend due to limited moisture supply. *Nature* 467:951–954
- Koren V et al (1999) A parameterization of snowpack and frozen ground intended for NCEP weather and climate models. *J Geophys Res* 104:19569–19585
- Koster RD et al (2004) Regions of strong coupling between soil moisture and precipitation. *Science* 305:1138–1140
- Koster RD et al (2006) GLACE: the global land-atmosphere coupling experiment. Part I: overview. *J Hydrometeorol* 7:590–610
- Law BE et al (2002) Environmental controls over carbon dioxide and water vapor exchange of terrestrial vegetation. *Agric For Meteorol* 113:97–120
- Lebel T, Ali A (2009) Recent trends in the Central and Western Sahel rainfall regime (1990–2007). *J Hydrol* 375(1–2):52–64
- Lee J, Pielke RA (1992) Estimating the soil surface specific humidity. *J Appl Meteorol* 31:480–484
- Liang X, Xie Z (2001) A new surface runoff parameterization with subgrid-scale soil heterogeneity for land surface models. *Adv Water Resour* 24:1173–1193
- Liang X et al (1994) A simple hydrologically based model of land surface water and energy fluxes for general circulation models. *J Geophys Res* 99:14415–14428
- Liang X et al (1996a) One-dimensional statistical dynamic representation of subgrid spatial variability of precipitation in the two-layer variable infiltration capacity model. *J Geophys Res* 101:21403–21422
- Liang X et al (1996b) Surface soil moisture parameterization of the VIC-2L model: evaluation and modification. *Global Planet Change* 13:195–206
- Liang X et al (1999) Modeling ground heat flux in land surface parameterization schemes. *J Geophys Res* 104:9581–9600
- Llovel W, Becker M, Cazenave A, Cretaux JF, Ramillien G (2010) Global land water storage change from GRACE over 2002–2009; Inference on sea level. *C R Geosci* 342:179–188
- Lobell DB, Burke MB (2010) On the use of statistical models to predict crop yield responses to climate change. *Agric For Meteorol* 150:1443–1452
- Mahfouf JF, Noilhan J (1991) Comparative study of various formulations of evaporations from bare soil using in situ data. *J Appl Meteorol* 30:1354–1365
- Marshall M et al (2011) Combining surface reanalysis and remote sensing data for monitoring evapotranspiration in sub-Saharan Africa. *Hydrol and Earth Syst Sci* (in review)
- Milly PCD, Cazenave A, Gennero MC (2003) Contribution of climate-driven change in continental water storage to recent sea-level rise. *Proc Natl Acad Sci* 100:13158–13161
- Minobe S (2005) Year-to-year variability in the Hadley and Walker circulations from NCEP/NCAR reanalysis data. Kluwer Academic Publishers, Amsterdam, Netherlands
- Morton FI (1983) Operational estimates of areal evapotranspiration and their significance to the science and practice of hydrology. *J Hydrol* 66:1–76
- Nagol JR et al (2009) Effects of atmospheric variation on AVHRR NDVI data. *Remote Sens Environ* 113:392–397
- Nicholson SE et al (1990) A comparison of the vegetation response to rainfall in the Sahel and East Africa, using normalized difference vegetation index from NOAA AVHRR. *Clim Change* 17:209–241
- Nijssen B et al (2001a) Predicting the discharge of global rivers. *J Clim* 14:3307–3323
- Nijssen B et al (2001b) Global retrospective estimation of soil moisture using the variable infiltration capacity land surface model, 1980–93. *J Clim* 14:1790–1808
- Pedely J et al (2007) Generating a long-term land data record from the AVHRR and MODIS instruments. Paper presented at

- IGARSS. IEEE international in geoscience and remote sensing symposium
- Philip JR (1957) The theory of infiltration: 4. Sorptivity and algebraic infiltration equations. *Soil Sci* 84:257–264
- Philippon N et al (2007) Characterization of the interannual and intraseasonal variability of West African vegetation between 1982 and 2002 by means of NOAA AVHRR NDVI data. *J Clim* 20:1202–1218
- Qian T et al (2006) Simulation of global land surface conditions from 1948 to 2004. Part I: forcing data and evaluations. *J Hydrometeorol* 7:953–975
- Rodell M et al (2004) The global land data assimilation system. *Bull Am Meteorol Soc* 85:381–394
- Rosero E et al (2009) Evaluating enhanced hydrological representations in NOAH LSM over transition zones: implications for model development. *J Hydrometeorol* 10:600–622
- Sellers PJ et al (1996a) A revised land surface parameterization (SiB2) for atmospheric GCMS. Part II: the generation of global fields of terrestrial biophysical parameters from satellite data. *J Clim* 9:706–737
- Sellers PJ et al (1996b) A revised land surface parameterization (SiB2) for atmospheric GCMS. Part I: model formulation. *J Clim* 9:676–705
- Shapiro R (1987) A simple model for the calculation of the flux of direct and diffuse solar radiation through the atmosphere. Air Force Geophysics Lab, Hanscom AFB, MA
- Taylor KE (2001) Summarizing multiple aspects of model performance in a single diagram. *J Geophys Res* 106:7183–7192
- Tucker C et al (2005) An extended AVHRR 8 km NDVI dataset compatible with MODIS and SPOT vegetation NDVI data. *Int J Remote Sens* 26:4485–4498
- Verdin KL, Verdin JP (1999) A topological system for delineation and codification of the Earth's river basins. *J Hydrol* 218:1–12
- Vrieling A et al (2011) Variability of African farming systems from phenological analysis of NDVI time series. *Clim Change*. doi: [10.1007/s10584-011-0049-1](https://doi.org/10.1007/s10584-011-0049-1)
- Wang G, Eltahir EAB (2000) Ecosystem dynamics and the Sahel Drought. *Geophys Res Lett* 27:795–798
- Wang A et al (2008) Integration of the variable infiltration capacity model soil hydrology scheme into the community land model. *J Geophys Res* 113:D09111
- Wilks DS (1995) *Statistical methods in the atmospheric sciences—an introduction*. Academic Press, Inc., San Diego, CA
- Williams A, Funk C (2010) A westward extension of the warm pool leads to a westward extension of the Walker circulation, drying eastern Africa. *Clim Dyn* 37:2417–2435
- Xie P, Arkin PA (1997) Global precipitation: A 17-year monthly analysis based on gauge observations, satellite estimates, and numerical model outputs. *Bull Am Meteorol Soc* 78:2539–2558
- Xue Y et al (2010) Intercomparison and analyses of the climatology of the West African Monsoon in the West African Monsoon modeling and evaluation project (WAMME) first model intercomparison experiment. *Clim Dyn* 35:3–27
- Zeng N (2003) Drought in the Sahel. *Science* 302:999–1000
- Zeng N, Neelin JD (2000) The role of vegetation-climate interaction and interannual variability in shaping the African Savanna. *J Clim* 13:2665–2670
- Zeng N et al (1999) Enhancement of interdecadal climate variability in the Sahel by vegetation interaction. *Science* 286:1537–1540
- Zhao M, Running SW (2010) Drought-induced reduction in global terrestrial net primary production from 2000 through 2009. *Science* 329:940–943